Int. J. Electrochem. Sci., 13 **(2018)** 10859 – 10872, doi: 10.20964/2018.11.57

International Journal of
ELECTROCHEMICAL
SCIENCE
www.electrochemsci.org

Study on the Combustion Products of Dimethyl Silicone Oil as Anode Materials for Lithium Ion Batteries

Keqiang Ding[1, 3*], *Xiaomi Shi*[1], *Chenxue Li*[1], *Xiaojing Gao*[1], *Jingwei Han*[1], *Hui Wang*[3], *Hongmin Dou*[3], *Junqing Pan*[2,*]

[1] College of Chemistry and Materials Science, Hebei Normal University, Shijiazhuang, Hebei 050024, P.R. China
[2] State Key Laboratory of Chemical Resource Engineering, Beijing University of Chemical Technology, Beijing, 100029, China
[3] Hebei LingDian New Energy Technology Co., Ltd, Tangshan, Hebei, 064200, P.R.China
[*]E-mail: dkeqiang@263.net; jqpan@mail.buct.edu.cn

Received: 4 June 2018 / *Accepted:* 6 August 2018 / *Published:* 1 October 2018

For the first time, a novel finding, that the combustion products of dimethyl silicone oil can be used as the anode materials for lithium ion batteries (LIBs), was reported in this work. Namely, a proper amount of dimethyl silicone oil was burned at 800℃ in a muffle furnace for 2 h, leading to the formation of two kinds of products, namely, white particles (sample a) and black particles (sample b). And then, sample a was thoroughly mixed with sample b at the mass ratio of 1:1 generating a new kind of material (sample c). All prepared samples were respectively characterized by XRD, SEM and XPS. No typical diffraction peaks were found in all resultant XRD patterns which strongly indicated that all prepared samples were amorphous in nature. SEM images revealed that many large spherical particles were prepared in sample a, and sample b contained many irregular large blocky particles. The results of galvanostatic charge and discharge experiments indicated that the initial discharge capacities of sample a, b and c at 100 mA g^{-1} were 43, 41 and 68 mAh g^{-1}, respectively. Interestingly, after 50 cycles, the discharge capacities at 100 mA g^{-1} of sample a, b and c were 30, 48 and 44 mAh g^{-1}, respectively. Summarily, a novel way, i.e., burning the Si-contained organic substances to prepare anode materials for LIBs, was developed in this work, which was very meaningful to the development of LIBs anode materials.

Keywords: dimethyl silicone oil; burning; anode materials; lithium ions battery

1. INTRODUCTION

The main purpose of this work is to show the fact that the combustion products of dimethyl silicone oil can be used as LIBs anode materials.

Of late, the significant roles of anode materials in improving the LIBs performance have been urgently claimed by many anode materials-related researchers [1]. The reasons for developing novel kinds of anode materials to replace the present commercial graphite anode material can be summarized as follows [2], (1) Although graphite as a commercial anode material for LIBs has been achieved for many years, the lower theoretical capacity (372 mAh g^{-1}) of graphite has greatly limited its further applications especially when developing LIBs with higher power and energy density [3]. (2) The formation of Li dendrites on graphite surface was, particularly in the case of being overcharged, documented to be the main problem for generating safety issue like fire accidents and short circuit [4]. (3) The appearance of the so-called solid electrolyte interphase (SEI) layer on graphite was demonstrated to be disadvantageous to the electrochemical performance of a LIB [5]. Thus, developing novel kinds of anode materials to substitute graphite has become a hot topic in the LIBs anode materials-related research realms.

Recently, many novel kinds of LIBs anode materials have been developed with an intention to replace the current anode material of graphite [6]. However, the complicated preparation process and the poor electrochemical performance were commonly regarded as the major issues which severely hindered the final commercialization of these newly developed anode materials. In other words, developing novel kinds of anode materials for LIBs is still a hot topic in the LIBs research fields. Very recently, SiO_2 was also developed to be an anode material for LIBs mainly because of its higher theoretical capacity and abundant resources. For example, in 2012, Sohn's group [7] investigated the electrochemical performance of SiO_2 for LIBs, in which SiO_2 was prepared by a high energy mechanical milling (HEMM) method using quartz as the precursor. Wu and his coworkers [8] reported the synthesis of graphene-wrapped SiO_2 nanotube network for LIBs, in which the SiO_2 layer was fabricated via a modified Stöber method using tetraethyl orthosilicate (TEOS) as the silica precursor. Chen's group [9] successfully synthesized hollow porous SiO_2 nanocubes and systematically studied their anode performances for LIBs, in which SiO_2 was produced using tetraethyl orthosilicate (TEOS) as the starting materials by a sol-gel process. Ozkan's group [10] fabricated SiO_2 nanotubes via a facile two step hard-template growth method, in their works, the amorphous layer of SiO_2 was deposited onto the commercial AAO templates via vapor phase deposition through thermal degradation of PDMS in air under vacuum. To the best of our knowledge, till present, there is no paper reporting the preparation of SiO_2 via burning Si-contained organic substances.

In this work, a proper amount of dimethyl silicone oil (a very cheap chemical raw material) was burned at 800 ^{o}C for 2 h in a muffle furnace under air conditions. Interestingly, white particles were formed on the surface of the crucible, and black particles were produced at the bottom of the crucible. The white particles and black particles were denoted as sample a and b, respectively. The mixture containing sample a and b was nominated as sample c. The galvanostatic charge-discharge measurement results demonstrated that the initial discharge capacity of sample c was 68 mAh g^{-1} at 100 mA g^{-1}. Although the electrochemical performances displayed by the prepared samples were poor when compared to those of the present LIBs anode materials, a novel method for preparing SiO_2-based anode material for LIBs was really developed in this work, which probably can be applied in the large scale production of LIBs anode materials.

2. EXPERIMENTAL

2.1. Materials

Dimethyl silicone oil was purchased from Tianjin Chemical Reagent Co. Ltd. All electrochemical measurement materials, such as acetylene black, polyvinylidene fluoride, 1 M $LiPF_6$ electrolyte and the cells, were all bought from the Tianjin Lianghuo S&T Developing Co. Ltd. All chemicals were utilized as-received without any further purification.

2.2. Preparation of SiO_2-based LIB anode materials

A proper amount of dimethyl silicone oil was placed in a clean and well dried crucible, and then, this crucible was put in a muffle furnace which was heated at 800 ^{o}C for 2 h, and after the muffle furnace was cooled down to the room temperature, the prepared samples were harvested carefully. The white particles immobilized on the surface of the crucible were called as sample a (photo a in Fig.1a). The black particles left on the bottom of the crucible were collected as sample b (photo b in Fig.1a). And then, sample a and sample b were mixed totally at a mass ratio of 1:1 generating sample c (photo c in Fig.1a).

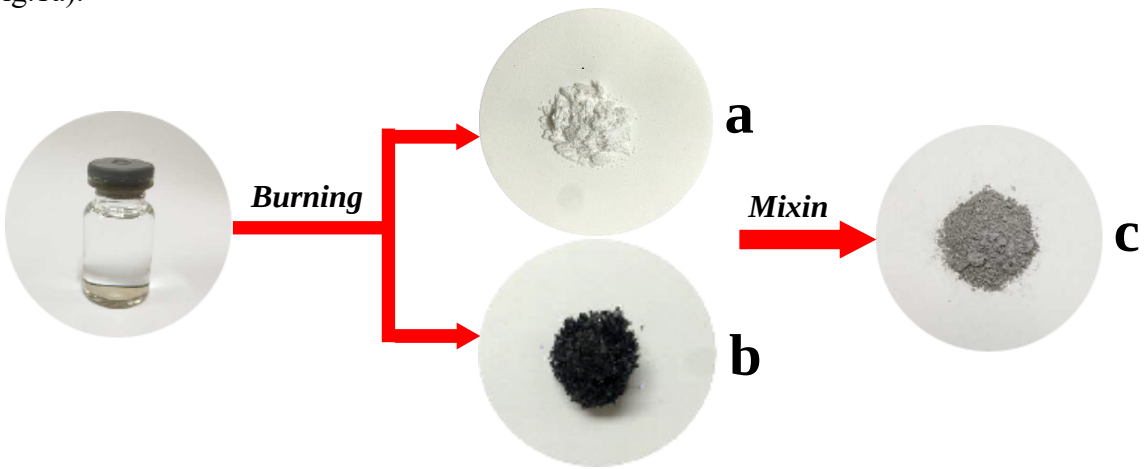

Figure 1a. Photos for the prepared samples. Photo a, b and c corresponded to sample a, b and c.

2.3. Characterization

The morphologies of all synthesized samples were carefully examined by scanning electron microscopy (HITACHI, SEM S-570) and transmission electron microscopy (HITACHI, TEM H-7650). The crystal structures of sample a and b were studied by using X-ray diffraction (Bruker AXS, D8 ADVANCE (Database version PDF-2004), Germany). The elemental compositions of the resultant samples were analyzed by employing energy dispersive spectrometer (EDS, INCA Energy 350, England). The elemental components and the chemical valences of detected elements were thoroughly characterized by X-ray photoelectron spectroscopy (XPS, Kratos Analytical spectrometer, Al K_{α} radiation).

The electrochemical measurements such as cyclic voltammetry (CV) and electrochemical impedance spectroscopy (EIS) were accomplished on a personal computer-controlled CHI 660B electrochemical workstation (Shanghai Chenhua Apparatus, China). In the EIS measurements, the amplitude of the alternating current (AC) and the frequency range were 5 mV and from 100 kHz to 0.1 Hz, respectively. All the experiments were conducted at room temperature.

The working electrodes were produced according to the following process. First, the resulting sample, acetylene black and polyvinylidene fluoride were milled together at a weight ratio of 8:1:1 leading to the formation of a new mixture. And then, several drops of N-methyl pyrrolidone (NMP) were carefully added into above mixture which was followed by a thorough stirring generating a cream. After that, the resultant creams were carefully pasted on a Cu foil using a glass piece, and then the produced sample was dried at 120℃ in a vacuum drying oven for 6 h. Approximately, the loading of the sample on each Cu foil was about 1.5 mg cm^{-2}. The half-cells, namely, the two-electrode cells, were assembled in a high pure nitrogen-contained glove box (ZKX type of Nanjing NANDA instrument factory) which mainly consisted of a lithium metal foil, an electrolyte of 1 M $LiPF_6$, Celgard 2400 separator and a working electrode. The solvent used was a mixed solvent which primarily contained dimethyl carbonate (DMC), ethylene carbonate (EC), ethyl methyl carbonate (EMC) and vinylene carbonate (VC). The metallic lithium foils were utilized as both the reference and auxiliary electrodes. The apparatus of CT-3008W-5V20mA-S4 (Shenzhen Neware Electronics Co., Ltd. China) was used to complete the galvanostatic charge-discharge measurements. The charge and discharge potential range was from 0.01V to 3 V, and the charging and discharging current density was identical to each other, being 100 mA g^{-1}.

3. RESULTS AND DISCUSSION

3.1 Morphology characterization

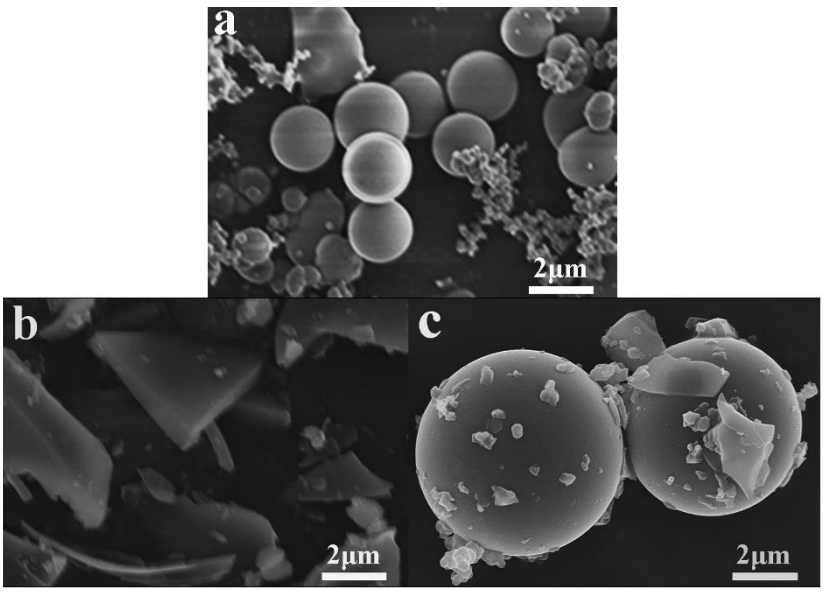

Figure 1b. SEM images for all prepared samples. Image a, b and c corresponded to sample a, b and c.

The SEM images of all resultant samples are presented in Fig.1b. Apparently, a lot of spherical particles with a size of 0.2-2μm were displayed in sample a, though some aggregates having much smaller particles were also observed clearly. This result strongly indicated that the white particles appearing in photo a (Fig.1a) were constructed by a plenty of spherical particles. Meanwhile, many huge irregular blocky-shaped particles were displayed in sample b. And evidently, the particle size of spherical particles in sample c was much larger than that of particles appearing in sample a. It seemed that after the milling process, some spherical particles in sample a were integrated to be large spherical particles, and these irregular particles appearing in sample b were rolled to be smaller particles. Generally, the differences in morphology may lead to different electrochemical performances of anode materials.

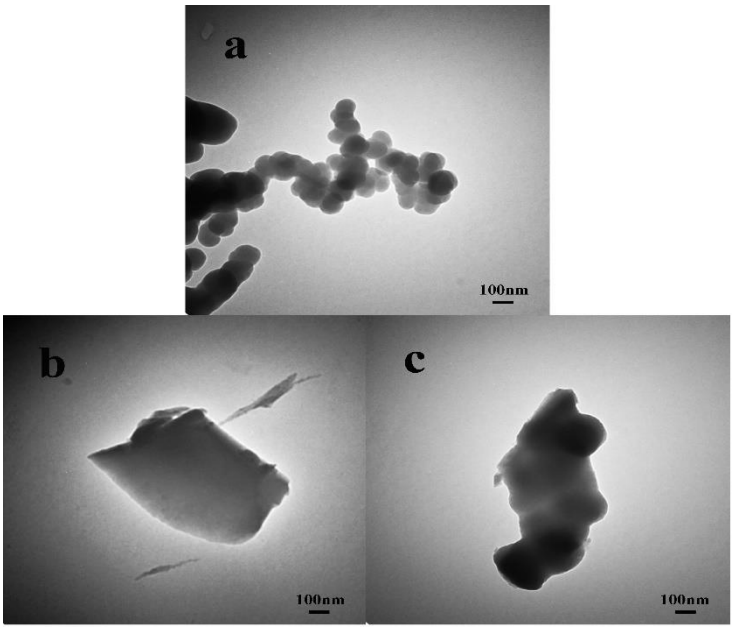

Figure 1c. TEM images for all prepared samples. Image a, b and c corresponded to sample a, b and c.

TEM images of all produced samples were also given in Fig.1c. For sample a, much smaller particles with a size less than 100 nm were displayed distinctly, which implied that these huge spherical particles in sample a (SEM image a in Fig.1b) were probably constructed by numerous smaller particles. As for sample b, irregular blocky-shaped particles appeared which agreed well with the morphology characterization results shown by image b of Fig.1b. In the case of sample c, it seemed that these smaller spherical particles were closely connected with each other forming irregular blocky-shaped particles.

3.2 XRD characterization

The XRD patterns for all produced samples including the standard XRD patterns of SiO_2 and Si are illustrated in Fig.2. All typical diffractions peaks corresponding to crystalline SiO_2 and Si were not displayed which indicated that the synthesized samples were amorphous in nature [9]. Meanwhile, a

broad diffraction peak positioned at around 22º appeared which just testified the presence of carbon based on our previous work concerning carbon nanotubes [11].

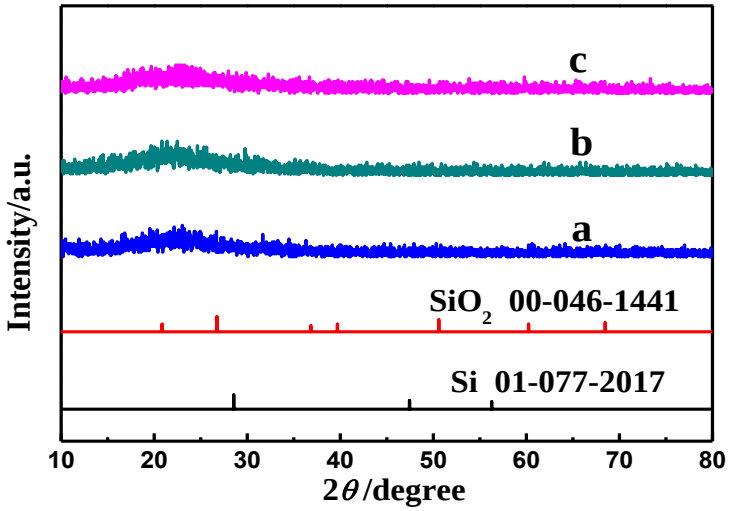

Figure 2. XRD patterns for all prepared samples. Pattern a, b and c corresponded to sample a, b and c. The standard patterns for SiO_2 and Si were also presented.

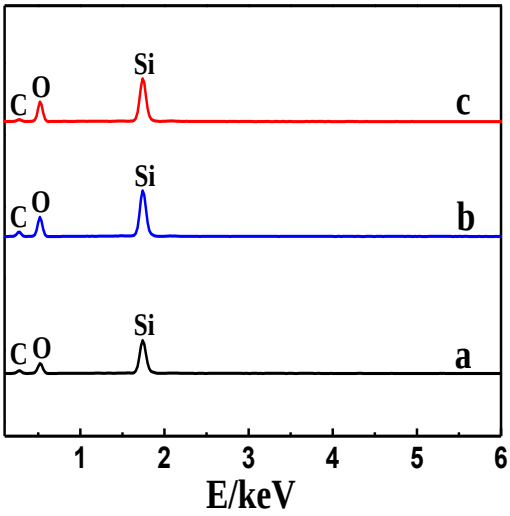

Figure 3. EDS patterns for all prepared samples. Pattern a, b and c corresponded to sample a, b and c.

The element compositions of all prepared samples were examined by using EDS measurement and the results are presented in Fig.3. For all produced samples, the peaks assigned to C, O and Si are definitely displayed, which suggested that no other impurities were contained in all resultant samples. The atomic contents of C, O and Si were 22%, 66% and 12% in sample a, 36%, 51% and 13% in sample b, 19%, 66% and 15% in sample c, respectively. That is to say, all prepared samples were a composite rather than a pure substance of SiO_2. The relatively higher content of carbon in sample b demonstrated that the main content of sample b was carbon, thus, the color of sample b was black.

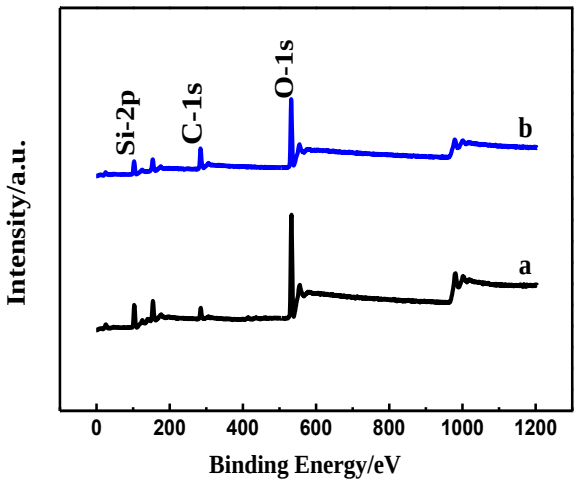

Figure 4a. Wide-scan XPS spectra for the prepared samples. Curve a and b corresponded to sample a and b.

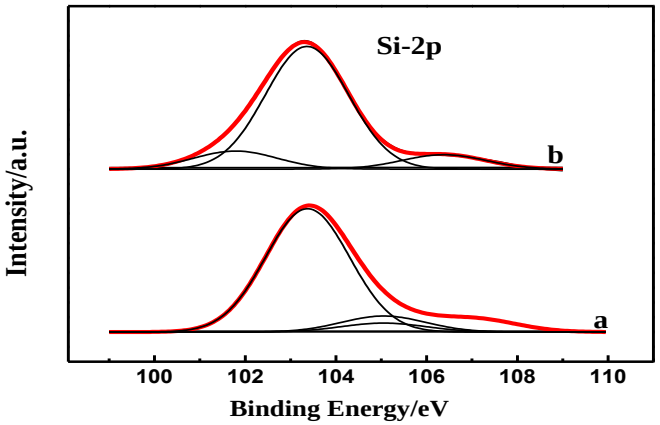

Figure 4b. High resolution XPS spectra of Si for sample a and b. Curve a and b corresponded to sample a and b.

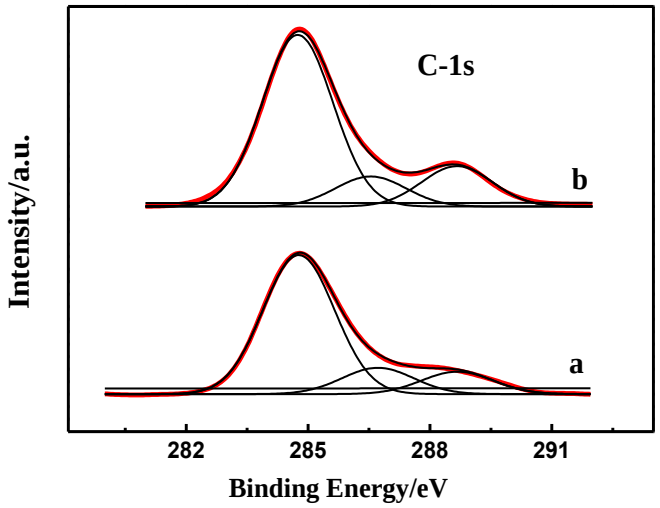

Figure 4c. High resolution XPS spectra of C for sample a and b. Curve a and b corresponded to sample a and b.

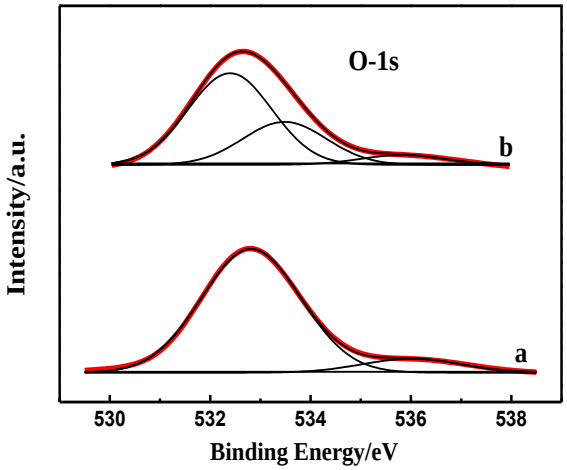

Figure 4d. High resolution XPS spectra of O for sample a and b. Curve a and b corresponded to sample a and b.

XPS measurement was also employed to study the element chemical valences of both sample a and b. Fig.4a clearly showed the lines of Si, O and C elements which agreed well with the results shown in EDS analysis (Fig.3). Fig. 4b displays the XPS spectra of Si 2P for sample a and b. By deconvoluting the spectrum of sample b, three chemical structures corresponding to the Si oxidation states were observed at BEs (binding energies) of 101.50 eV, 103.35 eV and 106.4 eV. The BE peaks appearing at 101.50 eV and 103.35 eV strongly, respectively, confirmed the presence of Si^{2+} and Si^{4+} in sample b based on the previous work [12]. Unfortunately, the explanation concerning the BE peak at 106.4 eV was not found which was probably due to the formation of silicon oxide with Si chemical valence higher than +4. In the case of sample a, only two peaks of at 103.35 eV and 105.3 eV were observed, and the peak at 101.50 eV totally disappeared which indicated the absence of Si^{2+} based substance. The presence of the huge peak at 103.35 eV in both sample a and b effectively documented that SiO_2 was main component in sample a and b. Fig. 4c illustrates the XPS spectra of C 1S for both sample a and b. Based on the former work [13], the component peak of at 284.8 eV should be attributed to the carbon atoms which do not connect with oxygen, and the peak of at 286.7 eV was originated from the carbon atoms only connecting with oxygen. The peak of at 288.7 eV was due to the presence of ether type carbon atom. Similar XPS curves were displayed in Fig.4c which strongly indicated that the chemical valences of carbon atoms in sample a and b were identical to each other. In the O 1s spectra (Fig.4d), two component peaks of at 532.4 eV and 535.9 eV were displayed by sample a, and three component peaks (532.4 eV, 533.5 eV and 535.8 eV) were presented in sample b. It was reported that the peaks at 532.4eV, 533.5 eV and 535.8 eV were respectively stemmed from the oxygen of C=O bond, the C-O single bond and the chemisorbed oxygen and water [14]. The difference in the XPS spectra for sample a and b strongly illustrated that the components of sample a and sample b were different from each other, which was consistent with the results of SEM (Fig.1b) and EDS (Fig.3).

3.3 Electrochemical properties

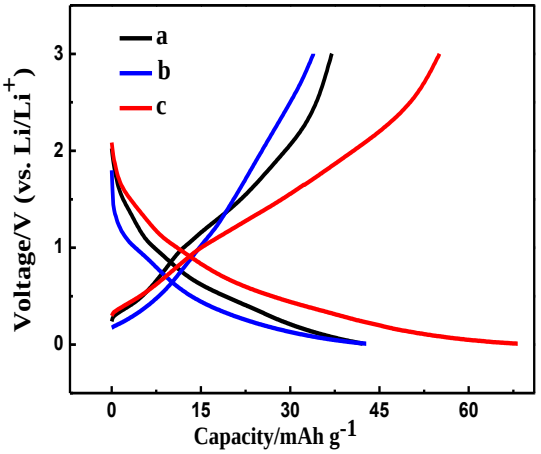

Figure 5. The initial charge and discharge profiles for all prepared samples. Curve a, b and c corresponded to sample a, b and c.

Fig.5 illustrates the initial charge-discharge profiles of all resultant samples at a current density of 100 mA g^{-1}. Apparently, sloped lines are observed in the charging and discharging process, and no flat voltage plateaus are displayed. The shapes of the charge-discharge curves were very similar to that of hard carbon SiO_2 electrode [15]. Thus, the sloped line in the discharge process appearing in 1.00-0.10V should correspond to the reduction of Si^{4+} and the formation Li-Si-O [15]. The charging voltage line appearing in 0.10-1.90V should correspond to the oxidation reaction of anode material which generally led to the formation of SiO_2 [15]. According to our previous works regarding electrode materials [16], when a pure two-phase transformation occurred in the charge-discharge process, there would be a very flat voltage plateau in the charging-discharging profile.

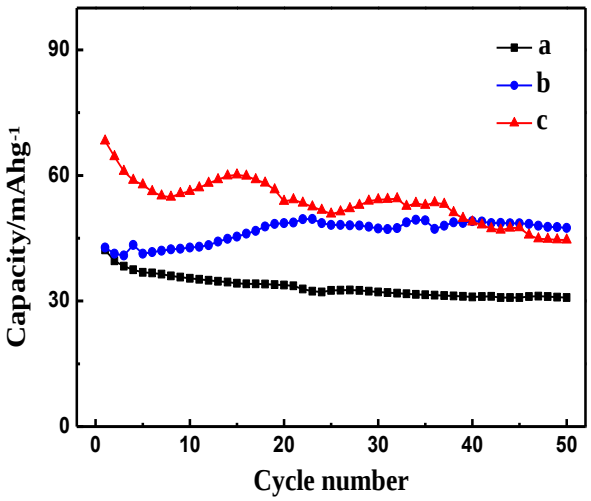

Figure 6. The curves describing the relationship between the discharge capacity and cycling number for all prepared samples. Plot a, b and c corresponded to sample a, b and c.

Therefore, the presence of the sloped voltage plateau in Fig.5 was probably due to the fact that

all prepared samples were a composite rather than a pure substance. The initial discharge capacities were, for sample a, b and c, approximately evaluated to be 43, 41 and 68 mAh g^{-1} at 100 mA g^{-1}, respectively. Namely, the largest discharge capacity was delivered by sample c, which was probably resulted from the presence of larger spherical particles (Fig.1b) when compared to that of sample a.

The cycling stability of an electrode material is closely related to the service life of a LIB [17], thus, the curves describing the relationship between the discharge capacity and the cycling number were also measured and illustrated in Fig.6. In the whole testing period, the discharge capacities for both sample a and c decreased evidently with the cycling number, for example, after 50 cycles, at the current density of 100 mA g^{-1}, the discharge capacities decreased from 42 to 31 mAh g^{-1} for sample a, and from 68 to 43 mAh g^{-1} for sample c, respectively. Thus, the capacity retention rates for sample a and c after 50 cycles were 74% and 63%, respectively. To our surprise, the discharge capacity of sample b slightly increased with the cycling number, for instance, the discharge capacities for the first and the 20th cycle were 42 and 47 mAh g^{-1}, respectively. This was a novel finding to our knowledge, which was probably due to the fact that some substances in sample b were reactivated to be lithium ions storage materials in the charge and discharge process. The results of Fig. 6 at least indicated that all prepared samples could be employed as anode materials for LIBs, though the discharge capacities delivered by the prepared samples were lower as compared to that of current LIBs anode materials.

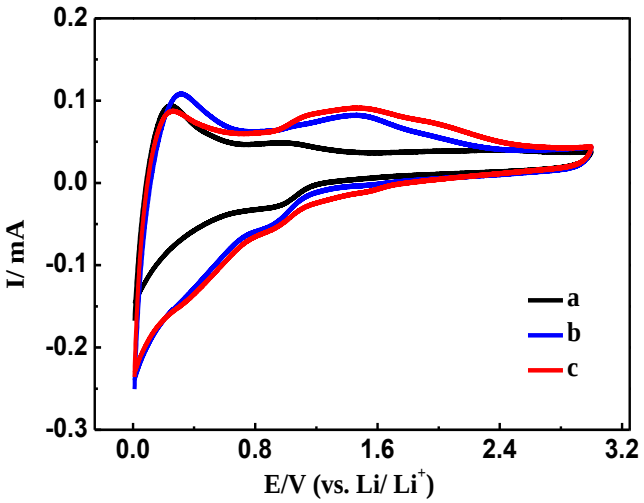

Figure 7. Cyclic voltammetry (CV) curves for all prepared samples which were recorded at the scan rate of 1mV s^{-1}. Curve a, b and c corresponded to sample a, b and c.

To further investigate the lithium ion insertion and extraction process in the prepared samples, the cyclic voltammetry (CV) curves of all produced samples are shown in Fig. 7. Generally, the oxidation peaks were attributed to be the presence of delithiation process, and the reduction peaks were originated from the lithiation process [17]. Thus, the presence of both oxidation and reduction peaks in the CV curves effectively certified the existence of lithium ion insertion and extraction process in all produced samples. According to the previous works concerning the Si and SiO_2 anode materials, the peak positioned at 0 V was attributed to the alloy-dealloy reaction of Si with Li ions [18], and the oxidation/reduction peaks delivered in the potential range of 0.9V-1.4 V were closely related to the

lithiation/delithiation process in SiO_2 [19]. In this case, for sample a (curve a), besides the redox peak at 0V, a broad and weak oxidation peak positioned at 0.99V and a reduction peak at 0.96V were observed clearly, strongly attesting the presence of lithiation/delithiation process in sample a. For sample b, two evident anodic peaks (at 0.31V and 1.47V, respectively) appeared in the positive-going potential scan, which also verified the existence of delithiation process in the charging process. Interestingly, in the negative-direction potential scan, three small reduction peaks (at 0.38V, 0.91V and 1.61V, respectively) were displayed, which just corresponded to the lithiation process in sample b. The CV curve shape of sample c was very similar to that of sample b, which implied that similar lithiation/delithiation processes were involved in sample c and sample b. Generally speaking, under the same conditions, the amount of electric charges consumed in an electrochemical reaction was in direct proportion to the peak area of a CV curve [20]. Obviously, in all prepared samples, sample c displayed the largest CV peak area, which was consistent well with the fact the largest discharge capacity was delivered by sample c (Fig.5).

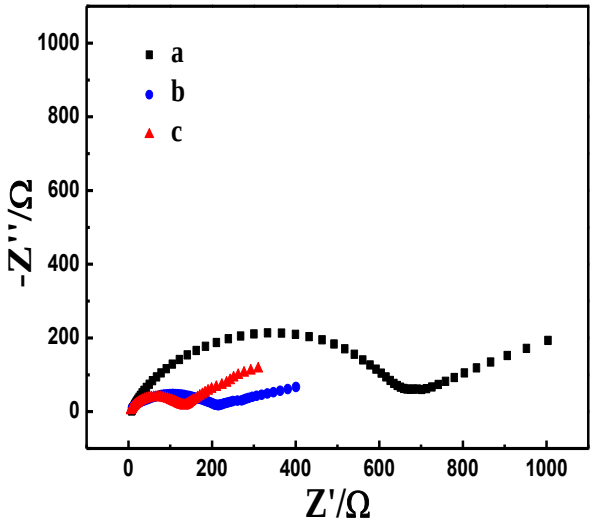

Figure 8a. Nyquist plots for all prepared samples which were recorded at their open circuit potentials. Curve a, b and c corresponded to sample a, b and c.

Nyquist plot (one typical curve of electrochemical impedance spectroscopy (EIS)), mainly due to its simple analysis, has been used as a regular curve to probe the electrochemical behavior of a lithium ion half-cell [16]. Fig. 8a illustrates the Nyquist plots of all prepared samples which were measured at their open circuit potentials. Evidently, all the Nyquist curves in Fig.8a showed similar shape which substantially documented that the mechanism of Li ions intercalation/deintercalation process in these samples was almost identical to each other. Based on our former works focusing on the LIBs electrode materials, the intercept appearing at the Z_{real} axis (here was Z') was mainly attributed to the total ohmic resistance (R_Ω), and the semicircle which appeared in the high-to-middle frequency range was commonly originated from the presence of a parallel circuit having a capacitive element and a resistor unit. The sloped line in the lower frequency region was nominated as the Warburg impedance which was closely related to the lithium-ion diffusion in the electrode materials [16]. According to the EIS data analysis, the value of the diameter for the semicircle appearing in the

high-to-middle frequency range was roughly equal to the value of the charge transfer resistance (R_{ct}), and a faster lithium insertion/extraction kinetics generally corresponded to a smaller value of R_{ct}. The values of R_{ct} for sample a, b and c were approximately estimated to be 660 Ω, 210 Ω and 132 Ω, respectively. Thus, sample c delivered the smallest value of R_{ct} among all prepared samples. That is to say, sample c had the fastest lithium insertion/extraction kinetics amongst the prepared samples, which just interpreted the fact that sample c had the largest discharge capacity among all the resultant samples (Fig.5).

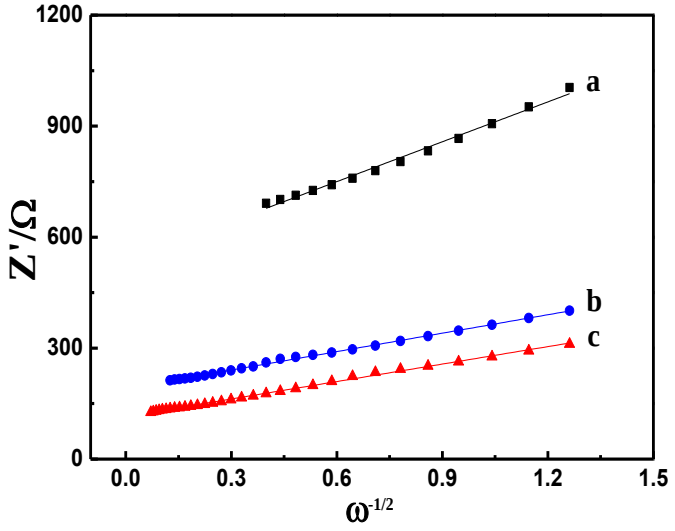

Figure 8b. Curves describing the relationship between Z' and $\omega^{-1/2}$. Curve a, b and c corresponded to sample a, b and c.

The parameter of Li-ion diffusion coefficient (D_{Li}) is also a key parameter via which Li-ion diffusion rates in various electrode materials can be compared directly. Commonly, the values of Li-ion diffusion coefficient were estimated using the following equation (1) [21].

$$D_{Li} = \frac{(RT)^2}{2(An^2F^2C_{Li}\sigma)^2} \qquad (1)$$

In above equation, A, n, C_{Li} corresponded to the surface area of the working electrode, the number of electrons transferred and the concentration of lithium ion in the anode materials, respectively. R, T and F had their own conventional scientific meanings. In this equation, σ (called as Warburg factor) was a new parameter which can be evaluated from the following equation [22].

$$Z_{re} = R_s + R_{ct} + \sigma \omega^{-1/2} \qquad (2)$$

In equation (2), Z_{re}, the real part of the impedance, was Z'. R_s was the resistance of electrolyte which was almost equal to zero here. R_{ct} and ω were the charge transfer resistance and the angular frequency in the lower frequency region, respectively. The curves describing the relationship between Z_{re} and $\omega^{-1/2}$ for all resultant samples were plotted in Fig. 8b, thus, the values of σ can be estimated directly from the slopes of these curves. However, the values of n and C_{Li} were unknown for these three newly prepared samples. Therefore, it was not possible to calculate the exact value of D_{Li} using

equations (1) and (2). To simplify the analysis, it was supposed that the values of both n and C_{Li} were identical in all prepared samples, thus, the values order of Li-ion diffusion coefficients could be compared approximately. Evidently, a smaller value of σ generally produced a larger value of D_{Li}. Therefore, the values of D_{Li} for these samples were in the following decreasing order, i.e., sample c> b>a. This result strongly demonstrated that it was easier for lithium ions to diffuse in sample c when compared to other samples, being consistent with the fact that sample c delivered the largest discharge capacity among all prepared samples.

4. CONCLUSIONS

For the first time, a novel method for preparing LIBs anode materials, namely, "burning" dimethyl silicone oil, was developed in this work. The results of EDS and XPS analysis indicated that all prepared samples were a SiO_2-contained composite rather than a pure substance. SEM images indicated that many spherical particles were produced in sample a and c. Electrochemical results indicated that the initial discharge capacity of sample c at 100 mA g^{-1} was 68 mAh g^{-1}. And after 50 cycles, the discharge capacity at 100 mA g^{-1} of sample c was maintained to be 44 mAh g^{-1}. Although the electrochemical performances exhibited by all prepared samples were not superior to that of the currently reported SiO_2 or Si-based anode materials, the work described here has really developed a new method to produce LIBs anode materials. That is to say, other metal oxides based LIBs anode materials can also be fabricated by this simple method, namely, burning metal-contained organic substance to prepare metal oxides anode materials for LIBs, which was the main contribution of this work.

ACKNOWLEDGMENTS
This work was supported by National Natural Science Foundation of China (21676022 & 21706004) and the State Key Program of National Natural Science of China (21236003), and the Fundamental Research Funds for the Central Universities (BHYC1701A & JD1701). This work was also financially supported by the Natural Science Foundation of Hebei Province of China (No. B2015205150) and the Technical Innovation Advanced Research Foundation of Hebei Normal University (L2018K03).

References

1. Y.-H. Kwon, K. Minnici, J.-J. Park, S.-R. Lee, G. Zhang, E.-S. Takeuchi, K.-J. Takeuchi, A.-C. Marschilok and E. Reichmanis, *J. Am. Chem. Soc.*, 140 (2018) 5666.
2. D. Sui, Y. Xie, W. Zhao, H. Zhang, Y. Zhou, X. Qin, Y. Ma, Y. Yang and Y. Chen, *J. Power Sources*, 384 (2018) 328.
3. Z. Wang, Y. Cheng, Q. Li, L. Chang and L. Wang, *J. Power Sources,* 389 (2018) 214.
4. Y. Deng, C. Fang and G. Chen, *J. Power Sources*, 304 (2016) 81.
5. H. Wang, X. Jiang, Y. Chai, X. Yang and R. Yuan, *J. Power Sources,* 379 (2018) 191.
6. X. Wang, H. Xue, Z. Na, D. Yin, Q. Li, C. Wang, L. Wang and G. Huang, *J. Power Sources,* 396 (2018) 659.
7. W.-S. Chang, C.-M. Park, J.-H. Kim, Y.-U. Kim, Go. Jeong and H.-J. Sohn, *Energy Environ. Sci.*, 5

(2012) 6895.
8. H. Wang, P. Wu, M. Qu, L. Si, Y. Tang, Y. Zhou and T. Lu, *ChemElectroChem,* 2 (2015) 508.
9. X. Liu, Y. Chen, H. Liu, Z.-Q. Liu and *J. Mater*. *Sci. Technol.*, 33 (2017) 239.
10. Z. Favors, W. Wang, H.-H. Bay, A. George, M. Ozkan and C.-S. Ozkan, *Sci. Rep.,* 4 (2014) 4605.
11. K. Ding, J. Zhao, Y. Chen, Y. Zhang, B. Wei and Q. Wang, *Int. J. Hydrogen Energy*, 41 (2016) 1134.
12. S. Kim, M.-C. Kim, S.-H. Choi, K.-J. Kim, H.-N. Hwang and C.-C. Hwang, *Appi. Phys. Lett*., 91 (2007) 103.
13. J. Dai, Z. Zhao, J. Zhai and L. Jiang, *Nucl. Instrum. Meth. B.*, 243 (2006) 38.
14. A.-M. Puziy, O.-I. Poddubnaya, R.-P. Socha, J. Gurgul and M. Wisniewski, *Carbon*, 46 (2008) 2113.
15. B. Guo, J. Shu, Z. Wang, H. Yang, L. Shi, Y. Liu and L. Chen, *Electrochem. Commun.*, 10 (2008) 1876.
16. K. Ding, H. Gu, C. Zheng, L. Liu, L. Liu, X. Yan and Z. Guo, *Electrochim. Acta*, 146 (2014) 585.
17. K. Ding, J. Zhao, J. Zhou, Y. Zhao, Y. Chen, Y. Zhang, B. Wei, L. Wang and X. He, *Int. J.Electrochem. Sc*., 11 (2016) 446.
18. W. An, J. Fu, J. Su, L. Wang, X. Peng, K. Wu, Q. Chen, Y. Bi, B. Gao and X. Zhang, *J. Power Sources,* 345 (2017) 227.
19. J. Meng, Y. Cao, Y. Suo, Y. Liu, J. Zhang and X. Zheng, *Electrochim. Acta,* 176 (2015) 1001.
20. K. Ding, P. Wang, J. Zhao, Y. Li,Y. Chen, Y. Zhang, B. Wei, Y. Sun and J. Pan, *Int. J. Hydrogen Energ*., 42 (2017) 9766.
21. A.-Y. Shenouda and H.-K. Liu, *J. Power Sources*, 185 (2008) 1386.
22. T.-F. Yi, H. Liu, Y.-R. Zhu, L.-J. Jiang, Y. Xie and R.-S. Zhu, *J. Power Sources*, 215 (2012) 258.